Lattice mobility and anomalous temperature factor behaviour in cytochrome *c'*

B. C. Finzel & F. R. Salemme*

Protein Engineering Division, Genex Corporation, 16020 Industrial Drive, Gaithersburg, Maryland 20877, USA

Atomic temperature factors (*B*-values) obtained from X-ray refinement experiments provide empirical estimates of protein mobility that have been correlated with both theoretical simulations of protein dynamics[1] and experimental studies of antibody reactivity[2,3]. The comparison of *B*-values with protein solution properties requires adjustment of the apparent atomic mobilities to compensate for the effects of the crystal environment[4–6]. Here we compare crystallographically independent subunits of the dimeric cytochrome *c'* from the bacterium *Rhodospirillum molischianum* to examine how lattice effects influence refined *B*-values. In addition to local effects on protein mobility at crystal contacts[4,5], we show that *B*-value differences up to 12 Å^2 between subunits result from lattice disordering effects that approximate to concerted rotations of the molecules about a crystal symmetry axis.

Ferricytochrome *c'* from *R. molischianum* is a dimeric haem protein composed of identical 128-residue polypeptide chains. The protein crystallizes in the orthorhombic space group $P2_12_12_1$ ($a = 56.6$, $b = 72.4$, $c = 75.4$ Å), with a dimer in the crystallographic asymmetrical unit[7]. The structure has been crystallographically refined to an *R*-factor of 0.19 for 30,533 reflections with $F > 2\sigma F$ to 1.67 Å resolution[8]. Independently refined subunits are related by a non-crystallographic dyad axis with an r.m.s. difference between corresponding α-carbon positions of 0.40 Å. Many detailed features of the subunits, including the equivalent situations of some 40 bound solvent molecules per monomer, are conserved despite differing environments in the crystal lattice.

Figure 1*a,b* plots mean residue *B*-value against sequence number for the two subunits of the native dimer. Comparison of the subunits yields a correlation coefficient of 0.82. This is similar to values reported for structures determined in different crystal forms[5,9] and is indicative of the extent to which *B*-value behaviour may reflect intrinsic protein dynamical properties[1,4]. Despite the similarities, monomer *B*-values differ by up to 30 Å^2 locally and by some 6 Å^2 overall (Fig. 1*c*). These variations between chemically identical subunits are attributable to their different environments in the crystal lattice.

Lattice interactions could potentially affect *B*-value behaviour in a variety of ways[6]. One result of the intermolecular interactions formed at crystal contacts is the localized immobilization of protein side chains or surface backbone loops. Consequently, the *B*-values of groups involved in such interactions may imply local mobilities that are substantially smaller than actually occur in solution. Previous studies have correlated the magnitude of such localized effects with solvent-accessible surface area in the crystal lattice[5,10]. Comparison of the mean residue *B*-values and fractional accessible surface areas[11] for the individual cytochrome *c'* subunits yields correlation coefficients (0.69 and 0.61, Fig. 1*a, b*) comparable to those observed previously[5,10]. A difference plot between monomers (Fig. 1*c*) shows that *B*-value and accessible area variations frequently correspond to alternative lattice contacts made by the two monomers in the asymmetrical unit. Nevertheless, differences between monomers correlate relatively poorly (0.35), in part resulting from an average difference of 6 Å^2 in subunit *B*-value that is uncorrelated with any overall difference in accessible surface area. As shown below, these variations reflect a second type of lattice effect that involves

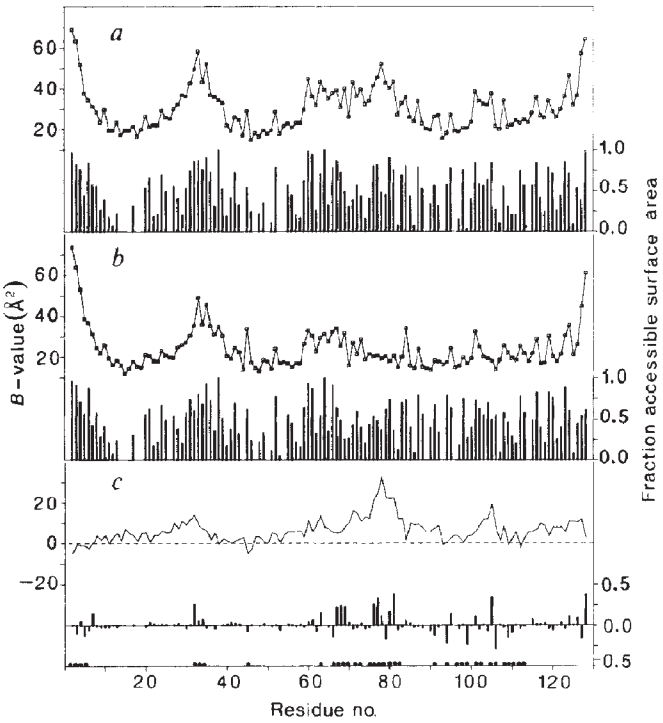

Fig. 1 *a, b*, Plots of residue *B*-value averaged over main-chain backbone atoms (connected curves), and fractional accessible surface areas[5,11] for entire residues in their respective crystal lattice environments (bars), against sequence number for crystallographically independent subunits of cytochrome *c'*. *c*, *B*-value (solid curve) and accessible surface area (bars) difference between subunits. Dots indicate sequence positions of residues that make different crystal contacts in the two subunits.

systematic disordering of molecules relative to crystal symmetry axes.

Figure 2 shows the crystal packing geometry and illustrates that subunits with sytematically low *B*-values (cool monomers) form continuous lattice interactions along alternate 2-fold screw axes parallel to the unit cell *c*-axis. Hot monomers make native dimer interactions with cool monomers aligned along each crystal screw, together with lattice contacts to cool monomers aligned along adjacent *c*-axis screws (Fig. 2*a*). Hot monomers interact only with cool monomers and are not in contact with each other in the crystal lattice. The crystal is thus organized as a parallel array of native dimer helices that are interconnected through hot monomer lattice interactions. This situation raises the possibility of systematic disordering of the hot monomers relative to the cool monomer arrays aligned along the *c*-axis crystallographic screws.

Figure 3 plots differences in mean *B*-value (ΔB) between corresponding residues of hot and cool monomers in the native dimer against their difference in radius (ΔR) from the *c*-axis crystallographic screw. This treatment compensates for variations in *B*-value that may arise from the local structural properties of the monomers (for example, extent of local secondary structure) and emphasizes differences that vary systematically relative to the crystallographic screw axis. The observed correlation (0.57) between ΔB and ΔR for dimer subunits indicates a continuous increase in average temperature factor for residues progressively more distant from the crystallographic screw. This behaviour is consistent with either static or dynamic lattice disordering phenomena involving rotational or wobbling displacements of the dimers relative to the crystal screw axis. The average behaviour (Fig. 3) suggests a maximum *B*-value contribution of 12 Å^2 at the hot monomer periphery resulting from extended lattice disordering effects. Assuming the simplest model involving rigid-body displacement of the dimer about the

* Present address: E. I. DuPont de Nemours Experimental Station, Central Research and Development Department, Wilmington, Delaware 19898, USA.

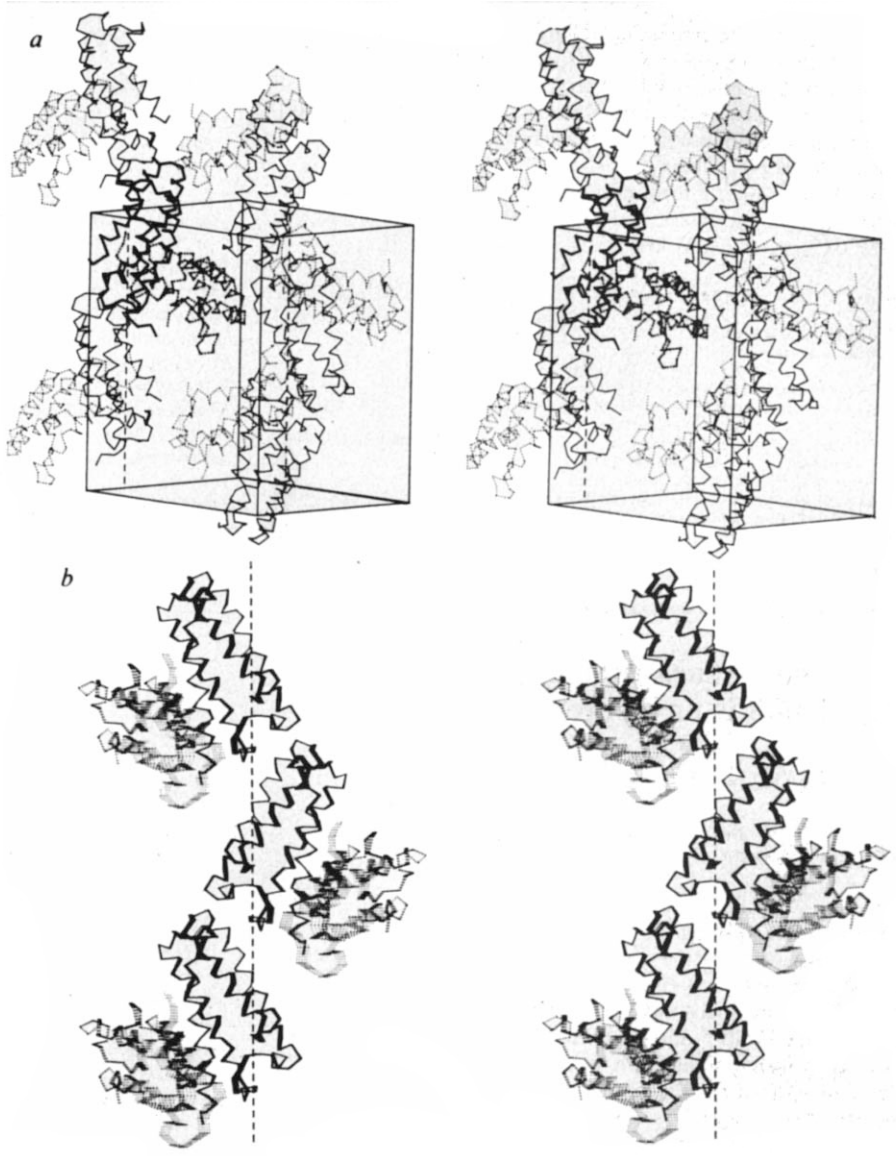

Fig. 2 *a*, Stereoview of the cytochrome *c'* crystal packing. Subunits (illustrated by α-carbon backbones) with lower average *B*-values (cool, solid) pack continuously along alternate 2-fold screws (long dashed) parallel to the unit cell (outlined) *c*-axis. Hot (dashed) monomers hold the lattice together by making native dimer (bold) interactions with each cool monomer array and lattice contacts with cool monomer arrays on adjacent screws. *b* Shows how the systematic *B*-value differences between monomers could reflect static or dynamic disordering involving rigid-body displacements of the molecular arrays about the *c*-axis screws. The observed *B*-value difference of 12 Å^2 at the hot monomer periphery (Fig. 3) suggests an axial rotation of 1.2° that produces a maximum displacement $U = 0.7$ Å, where $U^2 = 3B/8\pi^2$. The figure illustrates the superimposed effects of a rigid body rotation about the *c*-axis crystallographic screw that has been exaggerated by a factor of 3 for clarity.

crystallographic screw yields a corresponding r.m.s. amplitude of 0.7 Å (Fig. 2*b*).

The preceding experiment shows that observed differences in subunit *B*-factor behaviour in cytochrome *c'* result from a superposition of localized lattice packing effects that correlate with accessible surface area, and long-range disordering phenomena that reflect the extended pattern of molecular interactions in the crystal lattice. In the present case, the apparent motion may be related to a low-frequency vibrational mode of the V-shaped dimer, as suggested by the correlation (0.40) of monomer *B*-values with distance to the molecular dyad axis. Such concerted molecular flexing could produce the observed overall *B*-value behaviour, assuming that the cool monomers are relatively constrained in their aligned orientations along the *c*-axis crystallographic screws.

The comparison of protein structures determined in different crystal environments provides a basis for correcting *B*-values to account for the localized immobilizations that occur at crystal contacts[4,5], and thus allows estimates of protein dynamic flexibility in solution. Nevertheless, it is clear that extended lattice disordering effects, which may be unrelated to protein solution dynamics, can make comparable contributions to refined crystallographic *B*-values. It is anticipated that similar effects could occur in other high-resolution crystal structure determinations. However, such lattice effects could go unrecognized in the general case where the crystal asymmetrical unit contains only a monomer. In this case, the potentially non-uniform contributions to *B*-values from lattice disordering would be erroneously

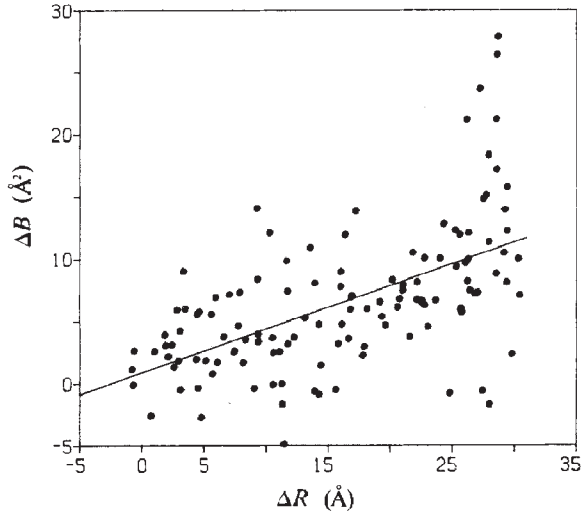

Fig. 3 Plot of the difference in mean backbone *B*-value (ΔB) between corresponding residues of the cytochrome *c'* subunits against their difference in radial distance (ΔR) from the crystal screw on which the cool monomers are aligned. The least-squares line suggests that the component varying systematically with ΔR contributes up to 12 Å^2 to the *B*-values of residues furthest from the crystal screw. Large deviations from the least-squares line correspond to residues forming different crystal contacts in the two monomer environments.

attributed to localized protein flexibility in solution. The significance attached to protein *B*-values, both in theoretical studies of protein dynamics[1] and practical applications of medical importance[2,3], justifies continued efforts at developing new theoretical and crystallographic refinement methods that can simulate crystal lattice effects.

We thank S. Sheriff for useful discussions and assistance with correlation plot software. This work was supported in part by NIHGMS grants 33325 and 30393.

Received 24 January; accepted 19 April 1985.

1. Karplus, M. & McCammon, J. A. *A. Rev. Biochem.* **53**, 263–300 (1983).
2. Westhof, E. *et al. Nature* **311**, 123–126 (1984).
3. Tainer, J. A. *et al. Nature* **312**, 127–134 (1984).
4. van Gunsteren, W. F. & Karplus, M. *Nature* **293**, 677–678 (1981).
5. Sheriff, S., Hendrickson, W. A., Stenkamp, R. E., Sieker, L. C. & Jensen, L. H. *Proc. natn. Acad. Sci. U.S.A.* **82**, 1104–1107 (1985).
6. Hartmann, H., Parak, F., Steigemann, W., G. A., Ringe Ponzi, D. & Frauenfelder, H. *Proc. natn. Acad. Sci. U.S.A.* **79**, 4967–4971 (1982).
7. Weber, P. C. *et al. Nature* **286**, 302–304 (1980).
8. Finzel, B. C., Weber, P. C., Hardman, K. D. & Salemme, F. R. *J. molec. Biol.* (submitted).
9. Artymiuk, P. K. *et al. Nature* **280**, 563–568 (1979).
10. Higuchi, Y., Kusunoki, M., Matsuura, Y., Yasuoka, N. & Kakudo, M. *J. molec. Biol.* **172**, 109–139 (1984).
11. Shrake, A. & Rupley, J. A. *J. molec. Biol.* **79**, 351–371 (1973).

Yeast heat-shock protein of M_r 48,000 is an isoprotein of enolase

Hidetoshi Iida & Ichiro Yahara

The Tokyo Metropolitan Institute of Medical Science, 3-18 Honkomagome, Bunkyo-ku, Tokyo 113, Japan

Exposure of cells or tissues of various living organisms to elevated temperatures induces the synthesis of a family of specific proteins called heat-shock proteins (HSPs)[1–3]. This phenomenon has so far been investigated mostly with respect to the induction mechanism of these HSPs[4,5]. However, little is known about the function of such proteins, although it has been suggested that they are involved in the acquisition of thermal tolerance[3]. We have recently suggested that a specific class of HSPs may function as negatively regulatory molecules in the growth of eukaryotic cells[6–8], and that a HSP of relative molecular mass (M_r) 48,000 (HSP48) from the yeast *Saccharomyces cerevisiae* may be involved in both thermal tolerance and growth control in this organism[8]. We now present evidence that *S. cerevisiae* HSP48 is an isoprotein of a glycolytic enzyme, enolase (EC 4.2.1.11). This unexpected finding may provide new insight into the role of the protein in the acquisition of thermal tolerance and growth control.

In *S. cerevisiae*, 6 out of 13 HSPs, including HSP48, are durably induced when cells are induced to enter the resting state of the cell cycle, G_0 (ref. 7). These G_0 yeast cells are much more resistant to heat shock than are growing cells, probably because of the accumulation of some or all of the above six HSPs. Induction of certain HSPs was also found with cultured cells of higher eukaryotes when they were arrested in G_0 (ref. 7). Furthermore, we have isolated a heat-shock-resistant mutant of the yeast which is defective in the *HSR1* gene and which constitutively synthesizes six proteins, including two isoforms of HSP48 (ref. 8). The *hsr1* mutant reveals unusual properties involved in growth control, in addition to the selected property that it is ~1,000-fold more resistant to lethal heat shock than the parental *HSR1* strain[8]. Because HSP48 is the only protein that is commonly induced in both growing *hsr1* cells and pre-heated or G_0-arrested *HSR1* cells, all of which are highly heat-shock resistant, we believe that HSP48 is responsible for the heat-resistance associated with these cells[8]. This is compatible with previous findings indicating that neither the products of the amplified *HSP90* genes[9] nor those of the two cloned genes of the *HSP70* family[10] are directly involved in the acquisition of resistance to lethal heat shock.

Table 1 Physicochemical and biochemical properties of HSP48 and yeast enolase

	HSP48	Enolase
Sedimentation coefficient ($s^\circ_{20,w}$)	5.3S	6.0S*
Stokes radius (Å)	36.5	36.2†
M_r from $s^\circ_{20,w}$ and Stokes radius	90,000	96,000
M_r from sedimentation equilibrium	84,000	88,000*
M_r from SDS-PAGE	48,000	48,000*
Enolase specific activity	69 ± 1	68 ± 1

Enolase activity was determined by monitoring the increasing rate of absorption at 240 nm at 25 °C as a result of conversion of D(+)2-phosphoglyceric acid (PGA) to phosphoenolpyruvate (PEP)[20]. Standard assay buffer consisted of 50 mM Tris-HCl (*p*H 7.8 at 25 °C), 2.7 mM magnesium acetate, 0.01 mM EDTA and 1.2 mM PGA. Specific activity is defined as the conversion of 1 μmol PGA to PEP per min per mg protein. Yeast enolase was a product of Oriental Yeast Co. Ltd, Tokyo.

* Data from ref. 21; † data from ref. 22.

Table 2 Amino-acid composition of HSP48 and yeast enolase

	HSP48	Yeast enolase
Asx	11.7	11.6
Thr	4.8	4.7
Ser	6.5	7.2
Glx	8.2	7.9
Pro	3.5	3.5
Gly	8.8	8.6
Ala	13.3	12.8
Val	7.4	7.9
Met	1.1	1.2
Ile	5.3	5.1
Leu	9.7	9.3
Tyr	2.1	2.1
Phe	3.7	3.7
His	2.4	2.6
Lys	8.2	8.6
Arg	3.2	3.3

Values are represented in mol%. Purified HSP48 was resolved in 7.5% SDS-PAGE[23]. The gel was not fixed or stained. Gel slices containing HSP48 were incubated in 0.02% SDS solution (1.0 ml per cm^3 gel) to elute the protein, and the elution was repeated. The combined eluates were extensively dialysed against distilled water for 2 days and lyophilized. The protein was hydrolysed in 6 M HCl at 110 °C *in vacuo* for 22 h and 70 h and analysed in an automatic amino-acid analyser (Hitachi model 835, Hitachi). Amino-acid composition of yeast enolase (peptide 1) was calculated from the amino-acid sequence of this protein deduced from the nucleotide sequence of the complementary DNA[12]. Cys and Trp residues were omitted from the above calculation as we did not determine the content of Cys or Trp in HSP48.

To elucidate the function of HSP48, extracts of yeast cells in the stationary phase underwent four successive purification steps and HSP48 was purified to homogeneity (see Fig. 1 legend). Purified HSP48 is composed of two isoforms, HSP48A (acidic form) and HSP48B (basic form)(Fig. 1*A*), as we have shown previously[7,8] by two-dimensional non-equilibrium *p*H gradient electrophoresis/SDS-polyacrylamide gel electrophoresis (NEPHGE/SDS-PAGE) of ^{35}S-methionine-labelled cells. Peptide mapping confirmed that the purified protein is identical to ^{35}S-methionine-labelled HSP48 (Fig. 1*B*).

We determined the N-terminal 23 amino acids of the purified HSP48 on a gas phase sequencer (Fig. 2). Using the Dayhoff protein sequence bank[11] to compare the sequence with those of other proteins, we found that the N-terminal 23 amino-acid sequence of HSP48 is identical to the corresponding sequence of yeast enolase (Fig. 2). In addition, physicochemical properties (Table 1) and amino-acid composition (Table 2) of the purified HSP48 were essentially the same as those of yeast enolase. Furthermore, the specific activity of the enolase in the purified HSP48 protein was the same as that of the authentic yeast